Lawrence Berkeley Laboratory
UNIVERSITY OF CALIFORNIA

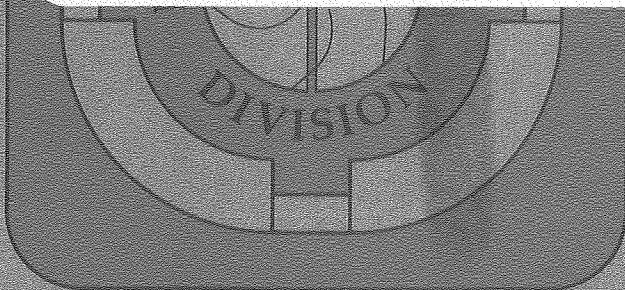Submitted to Physical Review C

ELECTROMAGNETIC DISSOCIATION OF RELATIVISTIC
^{18}O NUCLEI

D.L. Olson, B.L. Berman, D.E. Greiner, H.H. Heckman,
P.J. Lindstrom, G.D. Westfall, and H.J. Crawford

February 1981

DISCLAIMER

Electromagnetic Dissociation of Relativistic ^{18}O Nuclei*

D.L. Olson and B.L. Berman
Lawrence Livermore Laboratory, University of California
Livermore, CA 94550

D.E. Greiner, H.H. Heckman, P.J. Lindstrom, and G.D. Westfall
Lawrence Berkeley Laboratory, University of California
Berkeley, CA 94720

and

H.J. Crawford
University of California Space Sciences Laboratory
Berkeley, CA 94720

ABSTRACT

Measurements of fragment-production cross sections have been made with ^{18}O projectiles of 1.7 GeV/nucleon incident upon targets of Be, C, Al, Ti, Cu, Sn, W, Pb, and U at the LBL Bevalac. We have found that the enhancement with high-Z targets of cross sections for certain fragments agrees both in magnitude and Z_T dependence with the predictions of the electromagnetic-dissociation process, which are based upon the known photonuclear cross sections and classical relativistic virtual-photon theory. We have found as well that factorization of the cross sections for _nuclear_ processes is valid to an accuracy of better than 4%.

I. INTRODUCTION

There have been two previous experiments[1,2] in which the enhancement of fragment-production cross sections for high-Z targets was compared with the predictions of electromagnetic dissociation.[3] For both the experiment with ^{12}C and ^{16}O projectiles,[1] where the enhancement was noticed in the single-nucleon-loss channel, and the experiment with ^{56}Fe projectiles,[2] where the enhancement was seen in the Mn-fragment channel, the results were found to be consistent with these predictions. However, in themselves they do not constitute a compelling experimental verification of the electromagnetic dissociation of relativistic nuclei. A description of this process is given in Sec. II.

A beam of ^{18}O nuclei of energy 1.7 GeV/nucleon was chosen to provide a definitive test of the electromagnetic-dissociation process. For ^{18}O, in addition to the single-nucleon photonuclear channels, $\sigma(\gamma,n)$ and $\sigma(\gamma,p)$, there is a large two-neutron cross section, $\sigma(\gamma,2n)$. All of these cross sections were measured simultaneously at the Lawrence Livermore Laboratory Electron-Positron Linear Accelerator,[6] which lends great significance to the comparison of the relative magnitudes of the cross sections, σ_{em}. Also, the large ^{18}O$(\gamma,2n)$ cross section provides an important signature of an electromagnetic process. Finally, the magnitudes of the electromagnetic-dissociation cross sections for ^{18}O are comparable to the contributions from the competing nuclear processes.

In this experiment we measured the fragment-production cross sections for ^{18}O projectiles and the targets Be, C, Al, Ti, Cu, Sn, W, Pb, and U, for fragments ranging from ^{6}Li to ^{18}F with rigidity $4.8 < R < 6.3$ GV/c. These cross sections result from both nuclear and electromagnetic processes, and

we take them to be of the form

$$\sigma(T,F) = \sigma_{nuc}(T,F) + \sigma_{em}(T,F) \qquad (1)$$

(which assumes no interference between the nuclear and the electromagnetic processes). Because the calculated σ_{em} increases about 12% per fm increase in the overlap distance d (see Sect. II) and because of the high incident energy and the resulting forward trajectories this interference is expected to be small. This is equivalent to the electromagnetic-dissociation process being dominated by higher partial waves than those for the nuclear-fragmentation process, which is clearly the case.

Essential to our analysis is the factorization of the nuclear cross section,

$$\sigma_{nuc}(T,F) = \gamma_T \gamma_F \qquad (2)$$

where γ_T and γ_F are factors which depend only upon target and fragment, respectively.[7,8] These factors are determined empirically from a set of $\sigma(T,F)$, where $\sigma_{em}(T,F)$ is negligible. After the γ_T and γ_F have been determined they are applied in the appropriate combination to give $\sigma_{em}(T,F)$ from Eqs. (1) and (2).

II. THEORETICAL BACKGROUND

A. Calculation of cross sections

The electromagnetic dissociation of a relativistic nucleus (T $\sim$ GeV/ nucleon) is illustrated in Fig. 1 in comparison with peripheral fragmentation caused by nuclear processes. The electromagnetic-dissociation process occurs when a projectile nucleus passes near a high-Z target nucleus, but conceptually beyond the range of the nuclear force. The projectile is excited

by photoabsorption in the Coulomb field of the target nucleus, and then decays by particle emission.

In this experiment, the kinetic energy of the beam, ^{18}O at 1.7 GeV/nucleon, is more than two orders of magnitude greater than the Coulomb barrier for ^{18}O + U, which is $\sim$ 100 MeV. As a result, the electromagnetic dissociation investigated here is dominated by transverse photons, and the interference with nuclear processes is expected to be small.

A method of calculating cross sections for this process is indicated in Fig. 2 for the reaction ^{18}O + U $\rightarrow$ ^{17}O + n + U. By taking the product of a virtual-photon spectrum,[9] Fig. 2a, with the photoneutron cross section,[6] Fig. 2b, one obtains the differential-in-photon-energy cross section, Fig. 2c. At this point it is interesting to note that the low-energy part of this cross section is greatly enhanced and the high-energy part suppressed relative to the photoneutron cross section. Finally, we integrate this differential cross section to get the total electromagnetic-dissociation cross section

$$\sigma_{em}(T,F) = \int_0^\infty N_\gamma \sigma(\gamma,n) dE_\gamma \qquad (3)$$

where T and F stand for target (U) and fragment (^{17}O), respectively. In order to use the cross section measured with real photons in Eq. (3), we assume that the virtual-photon spectrum N_γ is the same for all multipolarities (see below). This is equivalent to the assumption that all of the photons are transverse.

B. Remarks on photon spectra

The two virtual-photon theories that we use are the Weizsäcker-Williams method of virtual photons from Jackson,[10] and a more sophisticated version of this method by Jäckle and Pilkuhn,[9] who derive spectra for various multi-polarities. The spectrum from Jackson is indicated by WW and is derived with the assumption of a point-charge target. The spectra from Jäckle and Pilkuhn are derived with the assumption of the target having a Yukawa charge distribution, and the resulting E1 and M1 spectra are indicated by JPE1 and JPM1, respectively. The spectrum from Jäckle and Pilkuhn for the case when the charge distribution of the target is taken to be a point charge[11] is indicated JPJ and ought to be equivalent to WW; however, it is not.

These spectra have one free parameter, b_{min}, which is the minimum impact parameter for the process. In our case, this is the impact parameter for which nuclear processes cease to dominate the interaction, and is the sum of the matter radii of the beam and target nuclei.

We simply quote the formulae for these spectra where Z_T is the charge of the target; γ, β are the usual relativistic factors; ω is the photon energy; $q_L = \omega/\beta$; $q_\ell = \omega/\gamma\beta$; $R = b_{min}$; the parameter for the Yukawa charge distribution is $a = \langle r_T^2 \rangle^{\frac{1}{2}}/\sqrt{6}$; $c^2 \equiv 1/a^2 + q_\ell^2$; and N is the photon spectrum in MeV^{-1}. The modified Bessel functions are denoted $K_{Li} = K_i(q_L R)$, $K_{\ell i} = K_i(q_\ell R)$, and $K_{ci} = K_i(cR)$. With this notation, the spectra are:

$$N_{WW} = \frac{Z_T^2 \alpha}{\omega \beta^2} \{ q_\ell R K_{\ell 0} K_{\ell 1} - \frac{1}{2} \beta^2 q_\ell^2 R^2 [K_{\ell 1}^2 - K_{\ell 0}^2] \} ;$$

$$N_{JPE1} = \frac{Z_T^2 \, \alpha R^2}{\pi \omega^3} \{q_\ell^2 q_L^2 \, [\, K_{\ell 0}K_{\ell 2} - K_{\ell 1}^2 - 2K_{L0}\frac{K_{\ell 2} - K_{\ell 0}}{1 - a^2\omega^2} \,]$$

$$+ \, q_\ell^4 \, (K_{\ell 1}^2 - K_{\ell 0}^2) + (q_L^4 + a^4\omega^4 c^4)\frac{K_{c1}^2 - K_{c0}^2}{(1 - a^2\omega^2)^2}$$

$$+ \, q_L^2 c^2 (1 + a^4\omega^4)\frac{K_{c0}K_{c2} - K_{c1}^2}{(1 - a^2\omega^2)^2} + \frac{4}{R} q_L^3 \frac{K_{L0} - K_{c0}}{(1 - a^2\omega^2)^2}K_{L1}$$

$$+ \, \frac{4}{R} ca^2\omega^2 (q_\ell^2 K_{\ell 0}K_{c1} + cq_\ell \omega^2 a^2\frac{K_{c0}K_{\ell 1}}{1 - a^2\omega^2} - q_L^2\frac{K_{L0}K_{c1}}{(1 - a^2\omega^2)^2})\} \; ;$$

$$N_{JPM1} = \frac{Z_T^2 \, \alpha}{\pi \omega} R^2 \{q_\ell^2 (K_{\ell 0}K_{\ell 2} - K_{\ell 1}^2) + c^2 (K_{c0}K_{c2} - K_{c1}^2)$$

$$- \, \frac{4c}{R} q_\ell a^2 (cK_{c0}K_{\ell 1} - q_\ell K_{\ell 0}K_{c1})\} \; ;$$

and for N_{JPE1} $(a = 0, \; c \to \infty)$ we have

$$N_{JPJ} = \frac{Z_T^2 \, \alpha R^2}{\pi \omega^3} \{q_\ell^2 q_L^2 [\, K_{\ell 0}K_{\ell 2} - K_{\ell 1}^2 - 2K_{L0}(K_{\ell 2} - K_{\ell 0})]$$

$$+ \, q_\ell^4 (K_{\ell 1}^2 - K_{\ell 0}^2) + \frac{4}{R} q_L^3 K_{L0}K_{L1}\}.$$

These spectra are shown in Fig. 3 for several beam energies. The following discussion will focus on the set for 10^3 MeV/nucleon in the region $10 < E_\gamma < 30$ MeV, which corresponds to the case most applicable to our experiment. One can see that N_{JPE1} (curve b) and N_{JPM1} (curve c) differ by about 10%. This, combined with the dominance of E1 transitions in the photonuclear cross sections, means that the assumption of equal multipolarities in Eq. (3) is quite good; the uncertainty introduced into the calculated σ_{em} by this assumption is less than the uncertainty in the measured photonuclear

cross sections. Another feature to be noted is that N_{JPJ} (curve d) is nearly identical to N_{JPE1}, differing by $\simeq$ 1%. This means that the size of the charge distribution in the target is of little importance. A bothersome feature is that N_{WW} (curve a) is larger than N_{JPE1} by 30 to 40%. Since this experiment is not sensitive to the exact shape of the photon spectrum, the only effect of this difference is to shift the value of b_{min} by $\sim$ 3 fm. This does not impair the main feature of our experiment; nevertheless, some work on the virtual-photon theory of relativistic nuclei is clearly needed.

These spectra have a factor Z_T^2, which gives the resulting electromagnetic-dissociation cross sections a strong dependence upon the charge of the target. However, there is some dependence upon Z_T in the parameter b_{min}, since a smaller value for Z_T yields a smaller value of b_{min}. As in Ref. 5 we define the overlap distance d by

$$b_{min} = R_{0.1}(B) + R_{0.1}(T) - d \qquad (4)$$

where B stands for beam and $R_{0.1}$ is the 10% charge-density radius. The 10% charge-density radii that we used in our calculations are listed in Table I. We expect $R_{0.1}$ to approximate the range of the nuclear interaction at these energies. By using d for our free parameter in place of b_{min} and calculating cross sections for a variety of targets with d held constant, we find the overall target dependence of σ_{em} to be

$$\sigma_{em}(T,F) = Z_T^{1.8} S(F,d) \qquad (5)$$

where S(F,d) contains all of the dependence upon the fragmentation channel and the effective range of the nuclear processes.

III. EXPERIMENTAL METHOD

The beam of ^{18}O accelerated by the Lawrence Berkeley Laboratory
Bevalac to 1.7 GeV/nucleon was incident upon the target in the spectrometer
shown schematically in Fig. 4. The target box, at one focal point, held the
nine thin 10.16-cm-diameter targets, whose characteristics are specified in
Table II. The quadrupoles were used to focus fragments of the correct rigidity
at the front of the detector telescope. The dipoles were set so that the
unscattered ^{18}O beam itself was deflected to the center of the "rail" upon
which the detector-telescope cart runs.

The detector telescope consisted of two Si(Li) wafers 0.2 mm thick by
45 mm in diameter followed by four thick Si(Li) detectors 5 mm thick by
44 mm in diameter. The two thin detectors were operated in coincidence for
the event trigger with the thresholds set to allow fragments with charge
$Z_F \geq 2$. The four thick detectors were used to measure ΔE, and hence the
charge ($\Delta E \propto Z_F^2$), of each fragment. All six of these detectors were coaxial.

The monitoring of the beam was carried out by the use of three detectors
plus a lead plate in the beam line behind the path of the cart and the two
secondary-emission monitors set off at $\pm 45^\circ$ to the side of and below the beam
and viewing the lead plate. The primary low-rate monitor was the particle-
mode counter (PC) in the beam. It was a pair of scintillator paddles operated
in coincidence which counted every beam particle for flux $< 10^6$ per one-second
beam spill. The primary high-rate monitor was the east secondary-emission
monitor (SEM). This also was a pair of scintillator paddles operated so
that they would have a coincidence for particles originating at the lead plate.
The SEM was used for the monitor for flux $> 10^6$ per one-second beam spill

and was calibrated against the PC at low rates. The other two detectors in the beam were an ionization chamber and a current-mode scintillator. These were used for cross checks of the other monitors and gave no indication that any problem developed with either the PC or the SEM. All of the scintillator paddles were 0.64 cm thick, and the PC and the SEM each had a scaler which was gated with the same "LIVE" signal as the charge-measuring telescope detectors.

On-line data acqusition was achieved through a CAMAC interface to a PDP 11/40 where the data were written first on a disk and then on a magnetic tape. The telescope detector was placed at 5-cm intervals over a range of 50 cm on the rail, symmetric about the beam position. There were roughly 30,000 events per run for the targets Be, C, Al, Ti, Pb, and U at each of the detector locations. The data for the targets Cu, Sn, and W were collected for only one value of rigidity, corresponding to the $Z_F/A_F = 1/2$ fragments.

IV. DATA ANALYSIS AND UNCERTAINTIES

The procedure for data reduction was (a) to calibrate the detectors for fragment charge, (b) to calibrate the beam monitors, (c) to compute the differential (in momentum) cross sections, (d) to fit these cross sections with a Gaussian form in order to get the fragment-production cross sections, (e) to correct for the transmission loss through the spectrometer in order to get the final values for $\sigma(T,F)$, (f) to determine the factors γ_T and γ_F, and (g) to derive the values for $\sigma_{em}(T,F)$.

A. Detector calibrations

Because the data were collected on an event-by-event, spill-by-spill, run-by-run basis, the calibrations could be made after the fact. Samples of

data from throughout the experiment were analyzed to determine the charge calibration for each of the four thick Si(Li) detectors. The charge-iden- tifivation procedure is illustrated in Fig. 5 for the $Z/A = 1/2$ fragments. Fig. 5a shows an example of a pulse-height spectrum. This spectrum was converted to a charge spectrum, shown in Fig. 5b, using a calibration of the form

$$Z_i = C_i \sqrt{D_i - D_{oi}} \tag{6}$$

where D_i is the ADC output of the ith detector for the event, C_i and D_{oi} are the calibration constants for the detector i, and Z_i is the calculated charge of the fragment. The constants C_i and D_{oi} exhibited no time dependence during the course of the experiment. In order to minimize the misidentification of fragments resulting from interactions in the detectors, the fragment-counting procedure required that each of the four detectors measured the same integer charge. Figure 5c shows a spectrum of the average of the calculated charges of the four detectors when this requirement is imposed. The systematic uncertainty introduced into the final cross sections by this calibration [Eq. (6)], is < 1%. The correction for proper counting of the fragments that do not pass the requirement mentioned above will be discussed below with the cross section formula.

The beam monitors were investigated and the SEM was determined to be the most reliable high rate monitor. It was calibrated using the PC with beam spills having less than 10^6 PC counts. The dependence of PC/SEM upon target and detector position (focusing) was investigated and no systematic target dependence was found. Therefore, the final calibration was averaged over runs with different targets at the same position, but was determined separately for each individual position. The systematic uncertainty resulting from this procedure is $\sim 3\%$.

B. Differential cross section

The differential cross section (in parallel momentum) is given by

$$\frac{d\sigma}{dp} = \frac{N(Z)\ (A/S_N)\ [(N_{evt} + n_p)/N_{evt}]}{SEM\ (PC/SEM)\ X_T N_T \Delta P} \tag{7}$$

where: - N(Z) is the number of fragments of charge Z that had the same integer

charge in each of the four detectors;

- A is the number of fragments whose average calculated charge is > 2.5;

- $S_N = \sum\limits_{Z=3}^{\infty} N(Z)$;

- $N_{evt} + n_p$ is the number of event triggers;

- n_p is the number of pile-up events, i.e., the number of events where a

second event trigger occurred before the computer had finished reading

the detectors and the "LIVE" signal returned;

- SEM is the number of counts from the secondary-emission monitor SEM;

- PC/SEM is the calibration of the SEM with respect to the particle

counter PC;

- X_T is the correction for beam loss in the target (1 + $\leqslant$ 0.05);

- N_T is the target thickness in atoms/cm^2; and

- ΔP is the momentum width of the detector.

Uncertainties in the term $(N_{evt} + n_p)/N_{evt} X_T N_T \Delta P$ introduce ~ 1% uncertainty into

the cross section. The pile-up correction usually was < 10%, and thus

introduces negligible uncertainty. The principal uncertainties here arise

from the correction for proper fragment counting and from the beam-monitor

calibration. As mentioned above, PC/SEM has ~3% systematic uncertainty,

independent of fragment charge, while the term A/S_N might conceivably have a

Z-dependent uncertainty. The purpose of the quantity A/S_N is to normalize

N(Z) to the actual number of charge-Z fragments (its value is typically 1.3).

The value used for A/S_N can err in two ways. First, when the number of

light fragments, e.g., Z = 2, 3, or 4, is a large fraction of the total number,

any charge misidentification that results from interactions in the detectors

or from electronic noise might cause A to differ from the correct number of

events with Z ⩾ 3. The uncertainty in $d\sigma/dp$ introduced by this depends upon

the relative numbers of fragments, but typically is $\sim$ 1% for Z ⩾ 5 fragments,

$\sim$ 2% for the Be fragments, and $\sim$ 3% for ^{7}Li fragments. Second, an uncertainty

in A/S_N comes about from the Z-dependent interaction rate in the detector

(from geometrical considerations alone). This results in a higher efficiency

for counting low-Z fragments in determining N(Z) than for counting high-Z

fragments. However, any electronic noise or base-level fluctuations in the

detectors would cause more losses for low-Z fragments than for high-Z fragments

because the pulse-height range for each charge unit is proportional to Z_F^2.

Analysis of the data yielded no noticeable Z-dependence in the counting

efficiency of N(Z) greater than 5%, and since A/S_N is weighted by the count

rate for a given charge, it is more accurate at the peak of a differential

cross section than in the tails of the distribution. The result of this

uncertainty in A/S_N is an uncertainty in the total cross section of $\sim$ 3%.

C. Total cross section

The differential cross sections were fitted by a least-squares minimi-

zation procedure using a Gaussian form[15] in parallel momentum

$$\frac{d\sigma}{dp} = \frac{\sigma_m(T,F)}{\sqrt{2\pi}\ \Gamma}\ \exp[-(P - \langle P \rangle)^2/2\Gamma^2]\ , \qquad (8)$$

a typical example of which is shown in Fig. 6. In many cases two cross sections were fitted simultaneously, as in Fig. 6. The fitting interval never spanned the range of rigidity which included that of the beam. The fitting parameters are (a) the measured total fragment-production cross section $\sigma_m(T,F)$, (b) the momentum width of the distribution Γ, and (c) the mean momentum of the distribution $\langle P \rangle$. This last parameter, $\langle P \rangle$, was constrained to be the same for each of the targets and depends only upon the fragment, except for the ^{16}O and ^{17}O fragments. For the ^{16}O and ^{17}O fragments, only $\langle P \rangle$ was constrained for the Be, C, Al, and Ti targets, while both Γ and $\langle P \rangle$ were constrained for the Pb and U targets; these latter constraints were independent of those for the set of light targets. This separation of Pb and U from the Be, C, Al, and Ti targets for the case of ^{16}O and ^{17}O resulted in a lower χ^2 for these fits and thus allowed us to take account of any possible influence of the electromagnetic-dissociation process on Γ and $\langle P \rangle$.

There is a systematic error in this fitting procedure in addition to the unknown (and presumably small) error in the assumption that these distributions are truly Gaussian. This error owes its origin to the significant momentum interval accepted by the detector, which has the effect of distorting the distribution. This was investigated and found to have a first-order effect on the measured width Γ but only a second-order effect on the total cross section $\sigma_m(T,F)$. This distortion is greatest for the heavy fragments, and could cause $\sigma_m(T,F)$ to be overestimated by 2 to 3% for $A_F \geqslant 16$, but its effect is less than 1% for $A_F \leqslant 15$.

Because of the narrow fitting interval used for the ^{6}Li-production cross sections and the fragment-counting correction mentioned above, the ^{6}Li-fragment cross sections contain a 20% target-dependent systematic uncertainty.

There were several cases for which there were not enough data to obtain the total cross sections from this fitting procedure. These are the Z/A = 1/2 fragments for the Cu, Sn, and W targets and the ^{16}N fragment for the rest of the targets (because of the proximity of the rigidity of the ^{16}N to that of the beam itself). For these cases, the transformation from a single $d\sigma/dp$ datum to the total cross section $\sigma_m(T,F)$ was obtained by analyzing the target dependence of the ratio $(d\sigma/dp)/\sigma_m$. The resulting cross sections contain a systematic uncertainty of $\sim$ 10% introduced by this latter procedure.

D. Transmission-loss correction

The correction for transmission loss through the spectrometer is of the form

$$\sigma(T,F) = X(\theta_F)\sigma_m(T,F), \qquad (9)$$

where the correction factor $X(\theta_F)$ depends upon the angle $\theta_F \equiv \Gamma_\perp/\langle P \rangle$; $\Gamma_\perp$ is the width of the Gaussian momentum distribution perpendicular to the beam direction and is assumed to be the same as the parallel-momentum width in the rest frame of the beam particles.[15] The measured momentum widths Γ were corrected for the effect of the momentum size of·the detector; this procedure introduced an uncertainty of $\sim$10% into the values for Γ. These widths then were transformed to the rest frame of the beam and were fitted with the Lepore-Riddell form[15,16]

$$\Gamma = \Gamma_o \sqrt{A_F(A_B - A_F)} / A_B, \qquad\qquad (10)$$

where A_B and A_F are the projectile and fragment masses, respectively, and Γ_o is the fitted parameter. The values for Γ_o that result from this procedure, together with the measured $\langle P \rangle$, were used to calculate θ_F. The correction for transmission loss is < 1% for $A_F \geqslant 15$, but increases rapidly with decreasing A_F, so that $X(\theta_F) = 1.77$ for ^6Li. The uncertainty in this correction is $\sim 10\%$ of $[X(\theta_F) - 1]$; thus it is negligible for $A_F \geqslant 13$, and it is $\sim 1\%$ for $A_F = 12$, but it becomes almost 10% for $A_F = 6$. It should be noted, however, that this uncertainty is independent of the target and hence γ_T, and therefore has no effect upon the electromagnetic-dissociation cross sections reported here.

E. Factorization and electromagnetic-dissociation cross sections

A set of 48 values for $\sigma(T,F)$ from eight fragments (^{15}N, ^{14}N, ^{15}C, ^{12}C, ^{12}B, ^{10}B, ^{10}Be, and ^7Li) and six targets (Be, C, Al, Ti, Pb, and U) were fitted with the form of Eq. (2) by a least-squares minimization procedure to produce the corresponding γ_T and γ_F. The γ_T for the targets Cu, Sn, and W were determined using the above γ_F from the fragments ^{14}N, ^{12}C, and ^{10}B. The γ_F for the electromagnetic-dissociation fragments ^{17}O, ^{16}O, ^{17}N, ^{14}C, and ^{13}C were determined with the above γ_T from the low-Z targets Be, C, and Al.

In order to estimate the accuracy with which these factors can be used to predict σ_{nuc} for target-fragment combinations that have a sizable σ_{em}, the ratio $r = \gamma_T \gamma_F / \sigma(T,F)$ was constructed for all the cross sections and analyzed in the following way. First, the values of r for the set of the 48 $\sigma(T,F)$ mentioned above were found to follow a Gaussian distribution with

a mean of $\bar{r}_1 = 1.003$ and a standard deviation of $\sigma_1 = 0.038$. The second analysis was performed on the values of r from a set of 77 $\sigma(T,F)$ which includes all of the measured $\sigma(T,F)$ except for those of the ^{6}Li fragment and for those with a sizable value for σ_{em}. The $\sigma(T,F)$ with a sizable σ_{em} are those for the fragments ^{17}O, ^{16}O, ^{17}N, ^{16}N, ^{14}C, and ^{13}C with the targets Ti, Cu, Sn, W, Pb, and U. These values for r were found to follow a Gaussian distribution with a mean of $\bar{r}_2 = 0.996$ and a standard deviation of $\sigma_2 = 0.044$. From this analysis, we conclude that the uncertainty in predicting σ_{nuc} for the purpose of determining σ_{em} from Eq. (1) is < 5% of σ_{nuc}. The uncertainty introduced into σ_{em} by this is dependent in turn upon the relative sizes of σ_{nuc} and σ_{em}.

After the target and fragment factors had been determined, they were used to predict σ_{nuc} via Eq. (2) in order that σ_{em} could be obtained from Eq. (1).

Folding together all of the above-mentioned uncertainties, including the factorization result, yields an overall systematic uncertainty in the values of σ_{em} from the Pb and U targets of $\sim$ 10% for ^{17}O and ^{16}O and $\sim$ 20% for ^{17}N, ^{16}N , ^{14}C, and ^{13}C.

V. RESULTS

The systematic behavior of the target dependence of the fragment production cross sections is shown in Fig. 7. This is illustrated for each fragment as the ratio of the cross section for each target to the cross section for the Be target. The points labelled γ_T, the target factors, are the result of averaging over eight fragments. The curve shown is a fit to the

γ_T data with the form indicated, as in Ref. 1. The points for the electro-magnetic-dissociation nuclei ^{17}O, ^{16}O, and ^{17}N show a striking deviation from this curve. With the assumption of factorization, (which is very good), the deviation of the points from the curve must be attributed to electro-magnetic dissociation. It is also clear from this picture that there is a strong dependence of this enhancement upon Z_T.

For the 48 values of $\sigma(T,F)$ used for the test of factorization, the fragments used in this fitting procedure (^{15}N, ^{14}N, ^{15}C, ^{12}C, ^{12}B, ^{10}B, ^{10}Be, and ^7Li) are all of the ones we measured (except for the ^6Li fragment, which has a target-dependent systematic uncerainty) for which there is no reasonable expectation of any electromagnetic-dissociation strength. The standard deviation of $\sigma_1 = 0.038$ for the values of r from these $\sigma(T,F)$ is most likely indicative of the experimental systematic uncertainties. Therefore, we can make the strong conclusion that nuclear factorization is valid with deviations of < 3.8%.

The electromagnetic-dissociation cross sections are listed in Table IV. The fragments for which we are able to calculate predictions (from the virtual photon spectra[9,10] and the measured photonuclear cross sections[6]) are shown in Table IV(a) and the cases for which predictions cannot be calculated (because the cross sections have not been measured) are shown in Table IV(b). Again the uncertainties listed are statistical only. The calculated predictions for the cross sections in columns JPE1 and WW contain an uncertainty from the photonuclear measurements of ~10% in addition to the uncertainty caused by the differences between the two photon

theories. The value of the overlap d used with the spectrum of Jäckle and Pilkuhn (JPE1) to compute the electromagnetic-dissociation cross sections is 1.5 fm, which gives the best fit to within 0.5 fm, considering the ^{17}O, ^{16}O, and ^{17}N data together. The corresponding value of the overlap used with the original Weizsacker-Williams (WW) theory to give the same fit is - 1.5 fm.

One can consider this experiment to be a measure of the overlap d, in which case the experimental uncertainties translate into an uncertainty of $\sim$ 1 fm in d. This can be compared to the skin thickness of nuclei, which is typically $\sim$ 2.2 fm. As can be seen in Table III, the measured values for σ_{em} for ^{16}O are relatively larger than those for σ_{em} for either ^{17}O or ^{17}N when compared to the theory. By fitting d to each of these three electromagnetic-dissociation channels individually, we find that the overlap distance to account for $\sigma_{em}(^{16}O)$ is about 2 fm larger than that for either $\sigma_{em}(^{17}O)$ or $\sigma_{em}(^{17}N)$. These results are shown in Table V. Because d is determined by <u>nuclear</u> processes (rather than by electromagnetic processes), the overlap for ^{16}O is consistent with the reasonable notion that two-neutron removal from the projectile is more likely to occur with a larger overlap (smaller impact parameter) than for single-nucleon removal.

The photodissociation cross sections appropriate to ^{16}N, ^{14}C, and ^{13}C have not been measured; thus predictions for σ_{em} for these fragments cannot be calculated. In consideration of both the results of a recent measurement at Giessen[17] of charged photoparticles from ^{18}O and those of the Livermore[6] measurement, the σ_{em} we determined are reasonable (see below).

In order to show the dependence upon Z_T of the electromagnetic-disso-
ciation cross sections, we have plotted σ_{em} for ^{17}O, ^{16}O, and ^{17}N as functions
of $\log(Z_T)$ in Fig. 8. The lines drawn are the predictions given by the
calculation of Jäckle and Pilkuhn[9] from Table III, JPE1. By fitting the
Z_T-dependence of the ^{16}O cross sections, we find that $\sigma_{em}(T,^{16}O) \propto Z_T^{1.67\pm0.15}$,
in agreement with the theoretical value of $Z_T^{1.8}$ given in Eq. (3).

VI. DISCUSSION

The main feature to be noticed from the results of this experiment is
that the enhancement of the fragmentation cross sections for ^{18}O projectiles with
high-Z targets in a channel corresponding to an appreciable photonuclear cross
section is described very well by the electromagnetic-dissociation process,
in terms of both magnitude and dependence upon Z_T. Given a conservative estimate
for the experimental uncertainties, the relative sizes of the electromagnetic-
dissociation cross sections $\sigma_{em}(T,^{17}O)$, $\sigma_{em}(T,^{16}O)$, and $\sigma_{em}(T,^{17}N)$ are consis-
tent with predictions using the measured photonuclear cross sections. However,
the fact that the cross section for ^{16}O is relatively larger than those for
^{17}O and ^{17}N indicates that the effective impact parameter for the nuclear
processes that produce ^{16}O might very well be smaller than that for the production
of either ^{17}O or ^{17}N.

The Giessen experiment[17] on ^{18}O suggests that we should see a small
amount of ^{16}N, which, in fact, we do. They also made a measurement of the
$^{18}O(\gamma,\alpha_0)^{14}C$ cross section, at photon energies $E_\gamma > 19$ MeV, which does not
have enough strength to produce the amount of ^{14}C that we see. However,
because of the low threshold for the $^{18}O(\gamma,\alpha)$ reaction ($E_\gamma = 6.23$ MeV),

such cross section as exists for E_γ < 19 MeV (not measured in the Giessen experiment) is greatly enhanced by the energy dependence of the virtual photon spectrum (see Fig. 2). Also, the Livermore measurement[6] indicates that there might be some strength in transitions to excited states in ^{14}C which also is not included in the Giessen data. Therefore, we expect to see considerably more ^{14}C production than that attributable alone to the (γ, α_0) cross section above 19 MeV. Also, considering the relatively low threshold for the $^{18}O(\gamma, \alpha n)^{13}C$ reaction (E_γ = 14.4 MeV), which is only 2.2 MeV higher than the $^{18}O(\gamma, 2n)$ threshold, we are not surprised at the magnitude of σ_{em} for the production of ^{13}C.

The question of factorization of nuclear cross sections embodied in Eq. (2) is a topic in itself and is not treated extensively here. We merely want to state our very significant result that factorization is valid to an accuracy of better than 4%. This limit is smaller by a factor of four than the previous experimental result of Ref. 8.

Having established that the electromagnetic-dissociation process is the correct mechanism for the enhancement in fragment-production cross sections for high-Z targets where the photonuclear cross sections are large, it can be seen that this type of experiment provides information on all of the photodissociation channels simultaneously. The quality of this information, however, would be enhanced significantly by a better treatment of the virtual photon theory; the difference between the two theories[9,10,11] with a point-charge target is particularly annoying.

The acquisition of information about all of the photoreaction channels simultaneously is a unique feature of this method. Another unique feature of the method is that it permits the measurement of the photoreaction channels of <u>unstable</u> nuclei with lifetimes as short as $\sim$ 10 ns, by the use of secondary beams of β-unstable nuclei; this in turn expands by a large factor the number of nuclei (especially light nuclei) available for photonuclear studies.

ACKNOWLEDGEMENTS

FOOTNOTES AND REFERENCES

1. H.H. Heckman and P.J. Lindstrom, Phys. Rev. Lett. $\underline{37}$, 56 (1976).

2. G.D. Westfall, L.W. Wilson, P.J. Lindstrom, H.J. Crawford, D.E. Greiner, and H.H. Heckman, Phys. Rev. $\underline{C19}$, 1309 (1979).

3. Electromagnetic dissociation at relativistic energies is the same process that has been described previously with the name Coulomb dissociation (see refs. 1, 2, 4, 5, 9). Within the nuclear-physics community, the term Coulomb implies a longitudinal photon process, whereas this process is dominated by transverse photons. In order to minimize confusion, we have chosen to use the name electromagnetic dissociation.

4. G. Fäldt, Phys. Rev. $\underline{D2}$, 846 (1970).

5. X. Artru and G.B. Yodh, Phys. Lett. $\underline{40B}$, 43 (1972).

6. J.G. Woodworth, K.G. McNeill, J.W. Jury, R.A. Alvarez, B.L. Berman, D.D. Faul, and P. Meyer, Phys. Rev. $\underline{C19}$, 1667 (1979).

7. W.R. Frazer, L. Ingber, C.H. Mehta, C.H. Poon, D. Silverman, K. Stowe, P.D. Ting, and H.J. Yesian, Rev. Mod. Phys. $\underline{44}$, 284 (1972).

8. P.J. Lindstrom, D.E. Greiner, H.H. Heckman, B. Cork, and F.S. Bieser, Lawrence Berkeley Laboratory Report LBL-3650, 1975 (unpublished).

9. R. Jäckle and H. Pilkuhn, Nucl. Phys. $\underline{A247}$, 521 (1975).

10. J.D. Jackson, "Classical Electrodynamics", (Wiley, New York, 1975), 2nd ed., p. 719.

11. H. Pilkuhn, private communication to H. Heckman, (1975).

12. R. Hofstadter and H.R. Collard, in "Landolt-Bornstein: Numerical Data and Functional Relationships in Science and Technology", edited by H. Schopper (Springer, Berlin, 1967), Group I, vol. 2, p. 21.

13. I. Angeli and M. Csatlos, Nucl. Phys. $\underline{A288}$, 480 (1977).

14. H. Miska, B. Norum, M.V. Hynes, W. Bertozzi, S. Kowalski, F.N. Rad,

C.P. Sargent, T. Sasanuma, and B.L. Berman, Phys. Lett. 83B, 165 (1979).

15. D.E. Greiner, P.J. Lindstrom, H.H. Heckman, B. Cork, and F.S. Bieser, Phys. Rev. Lett. 35, 152 (1975).

16. J.V. Lepore and R.J. Riddell, Jr., Lawrence Berkeley Laboratory Report LBL-3086, 1974 (unpublished).

17. K. Bangert, U.E.P. Berg, G. Junghans, R. Stock, and K. Wienhard, Nucl. Phys. A (to be published).

FIGURE CAPTIONS

1. Schematic diagram of the fragmentation reaction $^{18}O + ^{238}U \rightarrow ^{17}O + n + ^{238}U$
    showing the process of peripheral fragmentation resulting from the nuclear
    force and the electromagnetic-dissociation process occurring in the Coulomb
    field of the target nucleus. Note that electromagnetic dissociation can
    occur over a wide range of impact parameters, much larger than the limit
    set by the range of the nuclear force.

2. Ingredients for the theoretical calculation of the electromagnetic disso-
    ciation cross section $\sigma_{em}(U,^{17}O)$ for ^{18}O at 1.7 GeV/nucleon. Part (a)
    shows the E1 virtual-photon spectrum $N_\gamma(d)$ of Ref. 9 for $d = 1.5$ fm
    ($b_{min} = 10.2$ fm). Part (b) shows the measured photoneutron cross section
    $\sigma(\gamma,n)$ for ^{18}O, from Ref. 6. Part (c) is the product $N_\gamma \cdot \sigma(\gamma,n)$, which is
    the differential-in-photon-energy electromagnetic dissociation cross
    section. This is integrated to produce $\sigma_{em}(U,^{17}O)$.

3. Virtual-photon spectra. The sets of curves are labeled according to
    beam energy, from 10 to 10^5 MeV/nucleon. These are calculated for a
    U target with $b_{min} = 11.6$ fm. Curve (a) is from Ref. 10, which we denote
    as WW. Curves (b), (c), and (d), from Refs. 9 and 11, are the E1, M1,
    and E1(point charge) spectra which we denote as JPE1, JPM1, and JPJ,
    respectively.

4. Spectrometer layout. The telescope-detector cart was movable along the
    4-m-long rail. Fragments were focused at the front of the telescope
    detector. Secondary-emission monitors were below the plane defined
    by the beam and the detected fragments.

5. Fragment-charge calibration. Part (a) shows a sample pulse-height spectrum from the leading 5-mm thick telescope detector. Part (b) show the charge spectrum for the same data set. Part (c) shows the spectrum of the average charge measured by each of the four detectors with the requirement imposed that each detector measure the same integer charge.

6. A typical two-Gaussian fit of the differential (in parallel lab momentum) fragment-production cross section for the ^{12}C and ^{13}C fragments of ^{18}O projectiles incident upon the Pb target. This fit has $\chi^2 = 3$ for two degrees of freedom. The uncertainties indicated are statistical only. Systematic uncertainties are discussed in the text.

7. Target dependence of the fragment-production cross-section ratios, $[\sigma(T,F)]/[\sigma(Be,F)]$. The target factor γ_T is obtained by averaging these ratios over eight different fragments. The curve is obtained by fitting the γ_T points with the form $\gamma_T \propto A_T^{1/3} + A_B^{1/3} + X$, where X is the fitting parameter. Note the enhancement for ^{17}O, ^{16}O, and ^{17}N fragments resulting from the electromagnetic-dissociation process. The uncertainties indicated are statistical only. Systematic uncertainties are discussed in the text.

8. Electromagnetic-dissociation cross section σ_{em} vs. $\log(Z_T)$. The curves are the calculated predictions from Table IV. The uncertainties indicated are statistical only. Systematic uncertainties are discussed in the text.

Table I. Nuclear charge radii[a]

	A_T	$R_{0.1}$ (fm)	$R_{0.1}A_T^{-1/3}$ (fm)
Target[b]			
Be	9.01	3.38	1.62
C	12.01	3.29	1.44
Al	26.98	4.14	1.38
Ti	47.90	4.97	1.37
Cu	63.55	5.38	1.35
Sn	118.69	6.42	1.31
W	183.85	7.35	1.29
Pb	207.20	7.73	1.31
U	238.00	7.92	1.28
Beam[c]			
^{18}O	18.0	3.74	1.43

[a] The nuclear skin thickness $\equiv R_{0.1}-R_{0.9}$ is typically 2.2 fm.

[b] $R_{0.1}$ obtained from Ref. 12 except for Be, Ti, and Sn, for which $R_{0.1}$ was obtained by normalizing $r^{2\ 1/2}$ from Ref. 13, with r = 1.34, 1.38, and 1.38 respectively.

[c] $R_{0.1}$ from Ref. 14.

Table II.   Target specifications[a].

Target	Z_T	A_T	thickness	
			g/cm^2	radiation lengths[b]
Be	4	9.01	0.339	0.0052
C	6	12.01	0.253	0.0059
Al	13	26.98	0.328	0.014
Ti	22	47.90	0.348	0.021
Cu	29	63.55	0.425	0.033
Sn	50	118.69	0.419	0.048
W	74	183.85	0.488	0.072
Pb	82	207.2	0.570	0.089
U	92	238.0	0.587	0.098

[a] All targets were 10.16 cm in diameter.

[b] From Particle Data Group, *Review of Particle Properties*, Lawrence Berkeley Laboratory Report No. LBL-100, (1978), p. 21.

Table III. ^{18}O Fragment-production cross sections at 1.7 GeV/nucleon (mb)

γ_T		1.000	0.991±0.013	1.212±0.015	1.432±0.022	1.564±0.047	1.879±0.052	1.850±0.050	1.945±0.029	2.003±0.028
Target		Be[a]	C[a]	Al[a]	Ti[a]	Cu	Sn	W	Pb[a]	U[a]
γ_F	Fragment									
0.52±0.04	^{18}F	0.53±0.03	-	-	-	-	-	-	-	1.03±0.08
46.54±0.59	^{17}O	41.4±1.1	46.68±0.97	59.61±0.73	75.3±2.4	-	-	-	226.6±2.3	234.0±3.7
32.69±0.40	^{16}O	31.57±0.62	32.65±0.61	41.16±0.71	53.2±2.4	59.3±2.6	88.7±3.5	111.1±3.8	128.7±2.0	139.7±1.3
28.42±0.24	^{17}N	28.25±0.32	28.40±0.31	34.69±0.55	40.25±0.72	-	-	-	75.5±1.6	82.0±1.2
21.41±0.44	^{16}N	20.15±0.60	22.73±0.87	27.8±1.1	33.3±2.0	-	-	-	54.4±4.3	54.2±5.0
55.04±0.70	^{15}N[a]	55.24±0.77	55.4±1.1	64.98±0.95	76.1±1.5	-	-	-	110.2±1.5	111.0±2.6
12.83±0.22	^{14}N[a]	13.40±0.26	12.85±0.26	14.87±0.38	18.23±0.60	20.6±1.0	24.2±1.1	22.9±1.0	24.19±0.50	25.89±0.55
3.78±0.08	^{15}C[a]	3.81±0.13	3.80±0.09	4.60±0.09	5.54±0.14	-	-	-	6.66±0.56	7.09±0.24
27.80±0.27	^{14}C	27.02±0.34	30.95±0.58	38.27±0.63	49.74±0.89	-	-	-	89.6±3.9	92.6±2.6
36.12±0.37	^{13}C	37.19±0.54	37.28±0.66	47.33±0.69	52.6±1.1	-	-	-	94.7±1.9	92.7±2.1
29.38±0.37	^{12}C[a]	29.31±0.41	28.22±0.47	34.13±0.54	40.81±0.87	44.7±2.1	53.2±2.2	55.4±2.1	59.4±1.2	61.76±0.78
8.46±0.18	^{12}B[a]	8.03±0.22	8.34±0.20	10.93±0.23	11.96±0.29	-	-	-	15.9±1.1	16.33±0.69
8.84±0.17	^{10}B[a]	9.68±0.85	9.02±0.20	10.93±0.25	13.21±0.29	14.0±0.8	17.8±1.0	16.7±0.9	16.43±0.42	16.75±0.38
10.61±0.13	^{10}Be[a]	10.86±0.16	10.49±0.16	13.03±0.18	15.52±0.26	-	-	-	19.82±0.40	20.64±0.31
23.51±0.42	^{7}Li[a]	22.53±0.34	23.15±0.52	30.67±0.65	34.0±1.5	-	-	-	46.8±1.3	48.3±1.4
-	^{6}Li	29.56±0.44	27.05±0.49	32.44±0.88	36.33±0.64	29.2±1.6	33.4±1.7	34.4±1.8	47.8±1.0	46.9±1.0

[a] Targets and fragments which were used in the test of factorization (see text).

Table IV. Electromagnetic dissociation cross sections (mb).

Fragment	Target	Measured σ_{em}	Calculated JPE1[a]	WW[b]
(a)				
^{17}O	Ti	8.7 ± 2.7	13.4	12.5
	Pb	136.0 ± 2.9	132.	135.
	U	140.8 ± 4.1	162.	167.
^{16}O	Ti	6.3 ± 2.5	5.8	5.4
	Cu	9.0 ± 3.5	9.4	9.0
	Sn	27.5 ± 4.0	24.0	23.7
	W	50.0 ± 4.3	46.1	46.8
	Pb	65.2 ± 2.3	53.9	55.2
	U	74.3 ± 1.7	66.1	68.1
^{17}N	Ti	-0.5 ± 1.0	2.9	2.4
	Pb	20.2 ± 1.8	23.3	23.8
	U	25.1 ± 1.6	28.5	29.2
(b)				
^{16}N	Ti	2.7 ± 2.1		
	Pb	12.7 ± 4.4		
	U	11.3 ± 5.1		
^{14}C	Ti	8.8 ± 1.1		
	Pb	33.7 ± 4.0		
	U	35.1 ± 2.7		
^{13}C	Ti	-1.6 ± 1.5		
	Pb	21.9 ± 2.4		
	U	17.6 ± 2.6		

[a] For d = 1.5 fm
[b] For d = - 1.5 fm

Table V. Best-fit overlap values (mb).

Fragment	$d^{a,b}$	
	JPE1	WW
^{17}O	1.0	-2.5
^{16}O	2.5	-0.5
^{17}N	0.5	-3.0
weighted[c] average	1.5	-1.5

[a] $d \equiv R_{0.1}(T) + R_{0.1}(B) - b_{min}$

[b] These values are calculated to the nearest 0.5 fm.

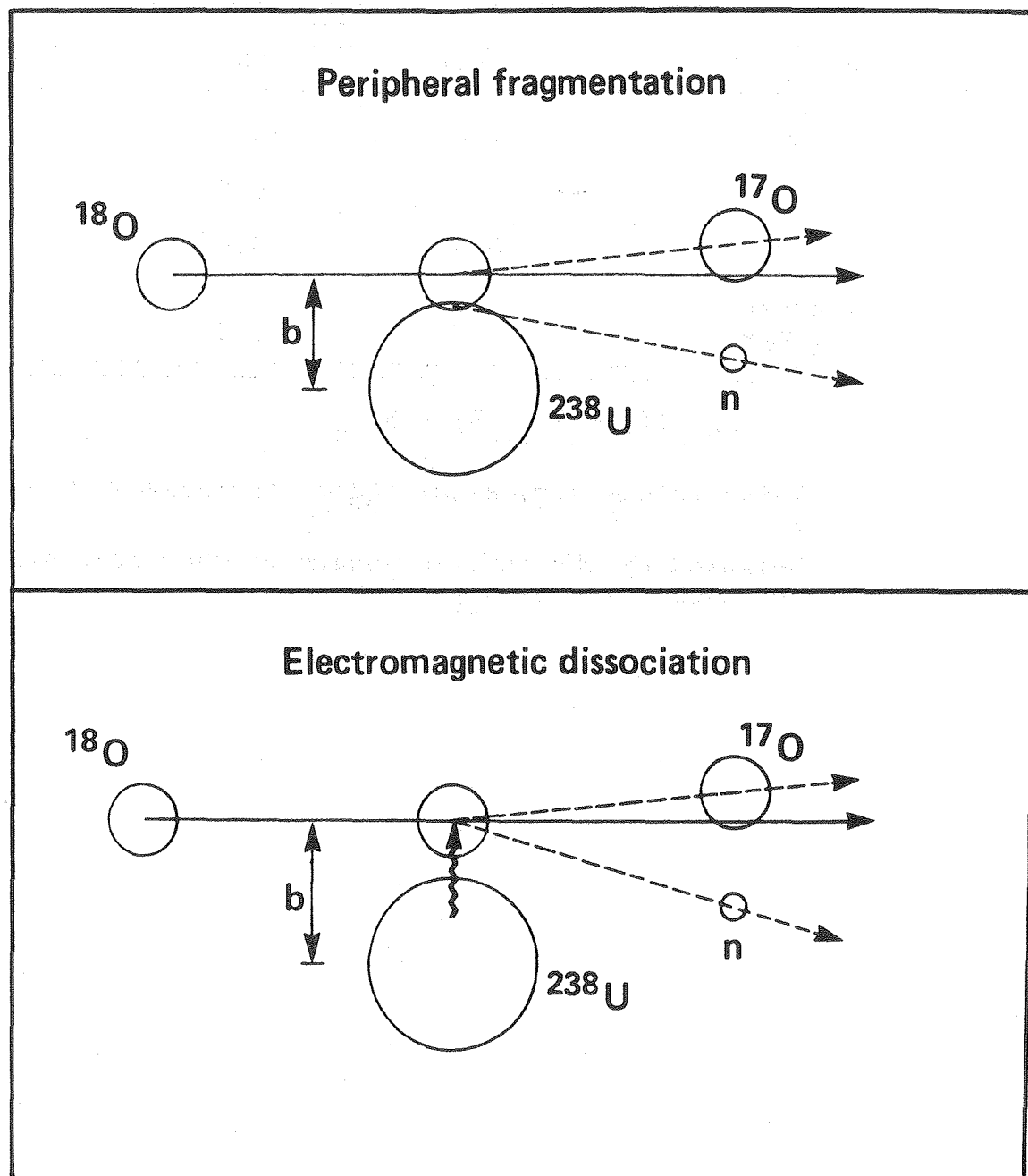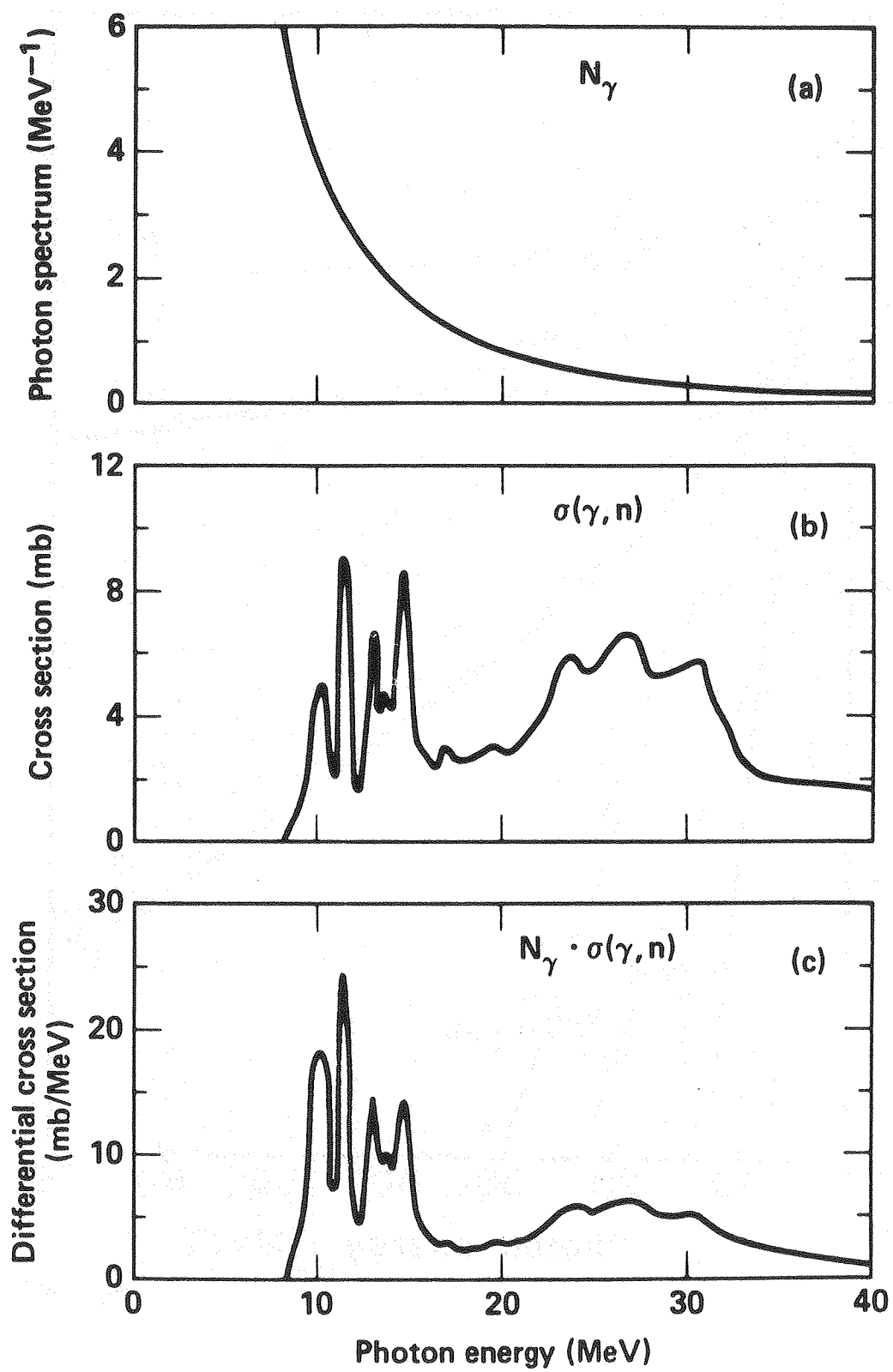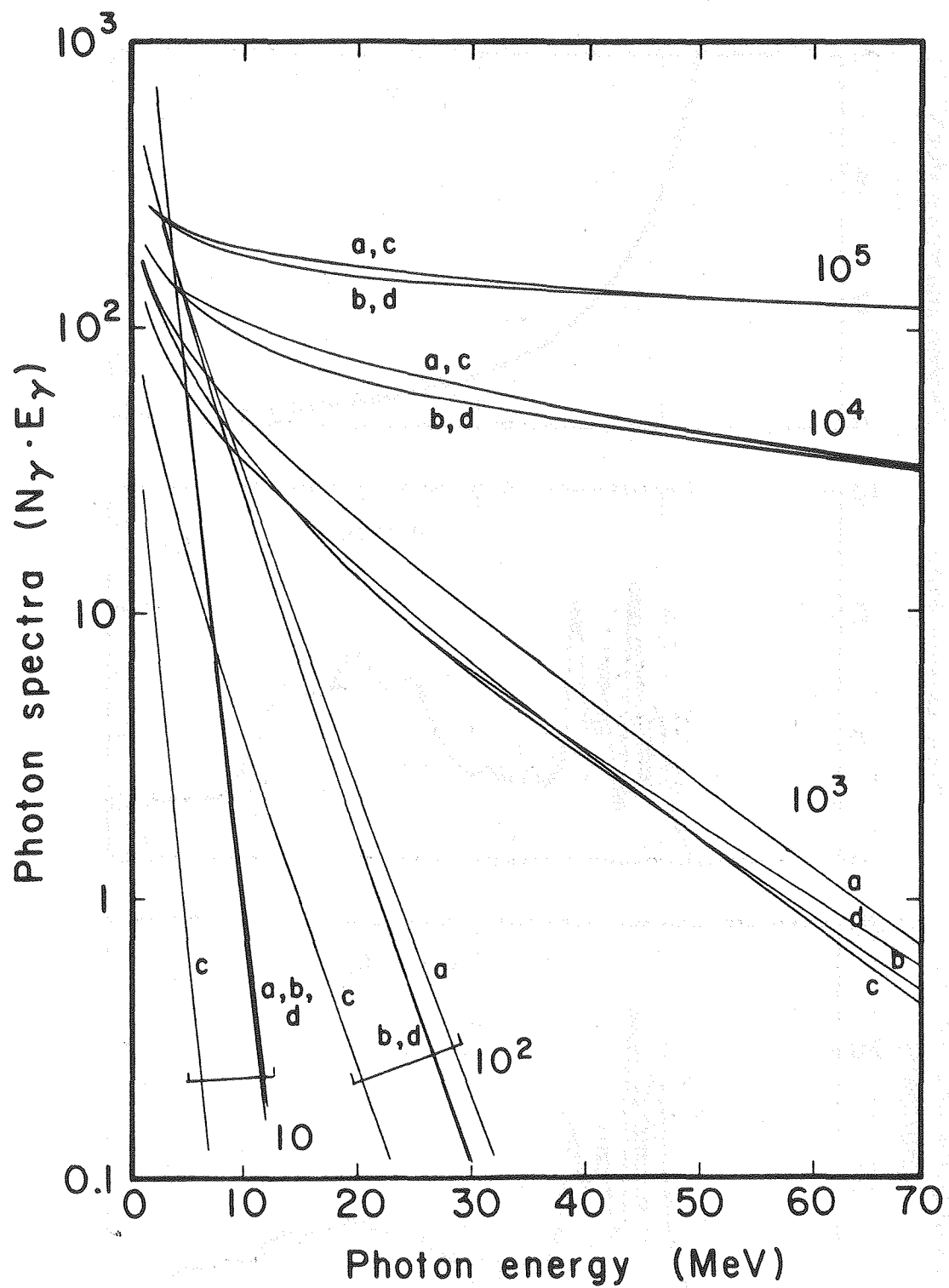[c] Weighted by the inverse square of the error bar for each value of σ_{em}.
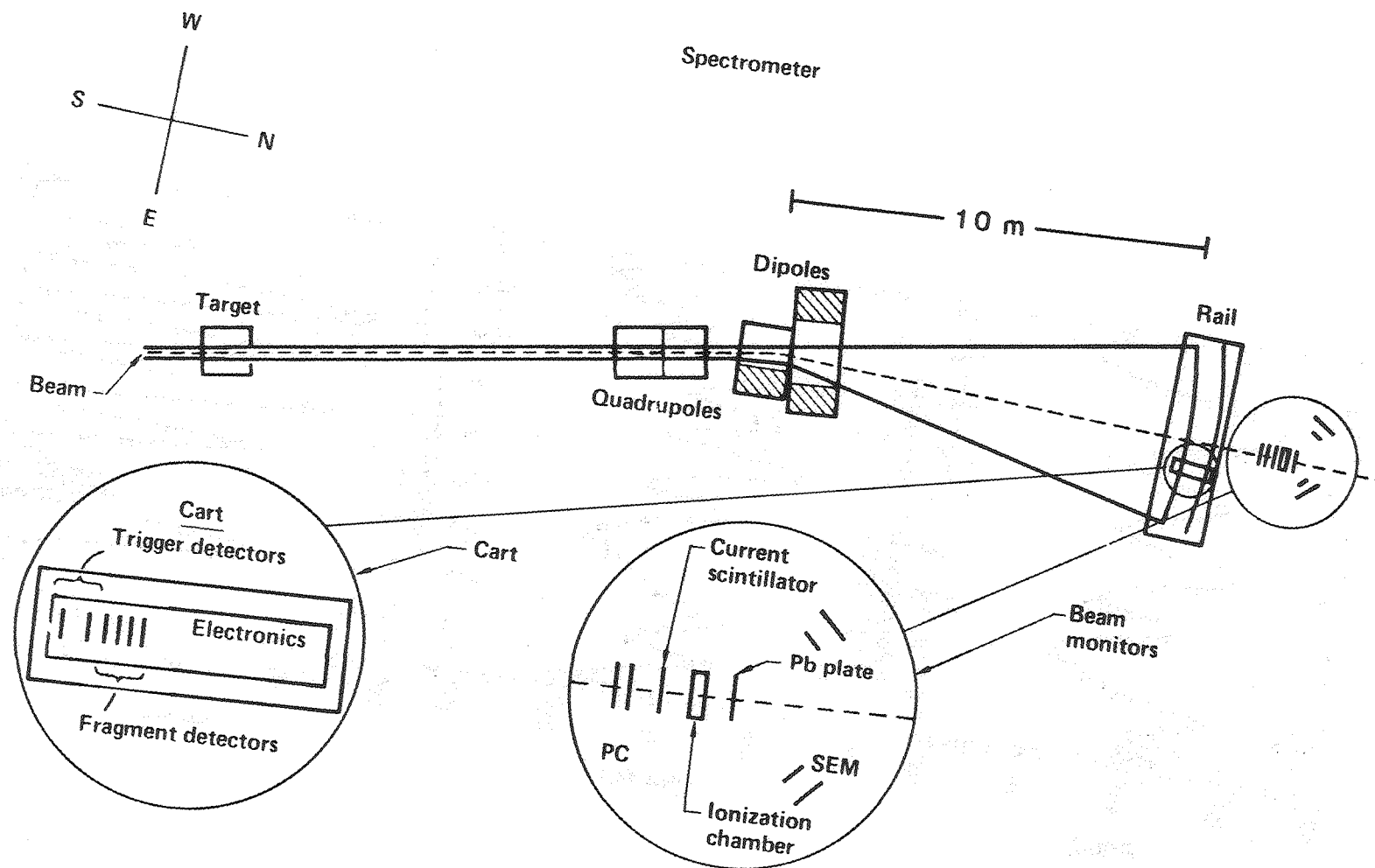
Fig. 1

Peripheral fragmentation

Electromagnetic dissociation

Fig. 2

Figure showing three stacked plots versus Photon energy (MeV):
(a) Photon spectrum N_γ (MeV^{-1})
(b) Cross section $\sigma(\gamma, n)$ (mb)
(c) Differential cross section $N_\gamma \cdot \sigma(\gamma, n)$ (mb/MeV)

Fig. 3

XBL 8011-7402

Fig. 4

Spectrometer

W

S

N

E

10 m

Dipoles

Target

Beam

Quadrupoles

Rail

Cart

Trigger detectors

Electronics

Cart

Fragment detectors

Current
scintillator

Pb plate

Beam
monitors

PC

SEM

Ionization
chamber

-33-

XBL 811-7671

Fig. 5

Fig. 6

$^{18}O + Pb \rightarrow Pb + C + x$

^{12}C

^{13}C

Differential cross section [mb/(GeV/c)]

Parallel momentum (lab frame) (GeV/c)

XBL 811-7670

Fig. 7

Fig. 8